catalysts

MDPI

Article

First Two-Way Electrochemical Sensor for the Detection of the Pollutant 2,4-Dinitrophenylhydrazine and Its Metabolite Based on Cu-Containing Tungstophosphate and Graphene Oxide

Xiaolei Yan, Xiaoxia Yu, Jianye Pei and Lihua Bi *

Department of Chemical Engineering and Applied Chemistry, College of Chemistry, Jilin University, Changchun 130021, China; yanxl21@mails.jlu.edu.cn (X.Y.)
* Correspondence: blh@jlu.edu.cn

Abstract: 2,4-dinitrophenylhydrazine (2,4-DNPH) is a toxic organic pollutant which is highly threatening to human beings and their living environment. Therefore, it is of great significance to develop sensors for detecting 2,4-DNPH and its metabolites. To develop a two-way electrochemical sensor for the detection of 2,4-DNPH and its metabolite, Cu-containing tungstophosphate ($Na_{16}P_4W_{30}Cu_4(H_2O)_2O_{112}{\cdot}nH_2O$, $Cu_4P_4W_{30}$) was selected to study its electrocatalytic activity for the reduction of 2,4-DNPH and oxidation of its metabolite. First, the electrochemical behavior of $Cu_4P_4W_{30}$ was investigated in solution; then, the films containing $Cu_4P_4W_{30}$ and graphene oxide (GO) were fabricated on indium tin oxide (ITO) to form the modified ITO/PDDA/$(Cu_4P_4W_{30}$/PDDA-GO$)_n$ electrode and the effect of the layer number on the electrocatalytic performance of the modified electrode was studied, confirming the optimal film layer number. Furthermore, the sensing performance of the modified electrode was tested, giving a linear concentration range and detection limit. Finally, the stability, repeatability, and reproducibility of the modified electrode were evaluated. The findings demonstrated that the proposed electrode acted as a two-way electrochemical sensor for the detection of 2,4-DNPH and its metabolite.

Keywords: tungstophosphate containing copper; modified electrode; electrochemical sensor; 2,4-dinitrophenylhydrazine; metabolite

Citation: Yan, X.; Yu, X.; Pei, J.; Bi, L. First Two-Way Electrochemical Sensor for the Detection of the Pollutant 2,4-Dinitrophenylhydrazine and Its Metabolite Based on Cu-Containing Tungstophosphate and Graphene Oxide. *Catalysts* **2023**, *13*, 769. https://doi.org/10.3390/catal13040769

Academic Editor: David Sebastián

Received: 23 December 2022
Revised: 13 April 2023
Accepted: 14 April 2023
Published: 18 April 2023

1. Introduction

2,4-dinitrophenylhydrazine (2,4-DNPH) is a red crystalline powder, belonging to the nitroaromatic and hydrazine family [1]. 2,4-DNPH is mainly used in the manufacture of explosives, pesticides, and foaming agents [2,3], but it has poor degradability and great poisonousness. It has been reported that hydrazine has neurotoxic, hepatotoxic, carcinogenic, mutagenic, and adverse health effects [4]. 2,4-DNPH can lead to oxidative damage to hemoglobin, resulting in a decrease in hemoglobin and carcinogenesis [5–7]. Due to poor degradability, 2,4-DNPH can be retained in the environment for a long time, posing a great threat to human health. It is of great significance to develop accurate and fast detection methods for the content of 2,4-DNPH in the environment. The reduction of 2,4-DNPH can produce its reduced product 2,4-diamino-phenylhydrazine called the metabolite of 2,4-DNPH, which still needs to be monitored. Therefore, it is necessary to explore a sensor that can detect both pollutants and their metabolites. Such a study will provide data to support the removal of the pollutant 2,4-DNPH completely from water and contribute an effort to obtain a clean water source.

To date, a series of detection methods of 2,4-DNPH have been explored, including chromatography [8], spectroscopy [9,10], titration [11,12], and photometry [13]. However, most of the methods have complex operation, long detection time, high price and requiring pretreatment. Compared to these methods, electrochemical technology has attracted more and more attention because of its irreplaceable advantages such as simple operation, fast

response, high sensitivity, wide detection range, low price, and environmentally friendly nature. Fortunately, a few examples of the electrochemical detection of 2,4-DNPH have been reported. Wang et al. fabricated poly(vinylpyrrolidone)-protected silver nanocubes (PVP–AgNCs) on GCE to prepare a sensor for the detection of hydrazine with a detection limit of 1.1 μM and wide linear range from 0.005 to 0.46 mM [14]. Boumya et al. used GCE to determine 2,4-DNPH in a divalent copper ion solution and obtained a linear range of 0.01 to 10 μM and a detection limit of 5.5 nM [15]; Adeosun et al. prepared a polyp-aminobenzoic acid-manganese oxide (P-pABA-MnO_2)-modified electrode to detect 2,4-DNPH, showing a linear range of 0.5 to 90 μm and a detection limit of 0.08 μM [1]. Recently, our group developed polyoxometalate-based electrochemical sensors to detect 2,4-DNPH, giving a wide linear range of 1 to 700 μM and a low detection limit of 0.012 μM [16]. This study indicates that polyoxometalates have a potential application as electrochemical sensors for the detection of 2,4-DNPH. Polyoxometalates (POMs), which are also called metal–oxo clusters, possess rich components and structures as well as excellent properties including acidity, conductivity, redox, catalysis, optics, and so on [17,18]. On the one hand, POMs have different negative charges; thus, they can be fabricated with the positive species to construct composite materials. On the other hand, POMs can participate in reversible multielectron transfer reactions without changing their original structures [19]. Moreover, transition-metal-substituted POMs not only add the redox characteristics of transition metal ions but also retain the high activity of original POM frameworks, thereby enlarging the application scope of POMs; for example, Mn, Ni-substituted POMs have been proved to electrocatalyze water splitting to generate hydrogen and oxygen [20,21]. The electrochemical behavior of Cu-substituted POM, $Cu_4P_4W_{30}$, was discussed in 2003 [22], showing a redox peak of a Cu and W-O framework, respectively. The structure of $Cu_4P_4W_{30}$ is represented in Figure S1, where Cu is called a coordination atom and W-O framework is considered the multidentate ligand, which coordinates with Cu ions to form the sandwich-type structure [23]. Cu ions have exhibited the electrocatalytic oxidation of 2,4-DNPH [15], whereas the W-O framework can electrocatalyze the reduction of 2,4-DNPH [16]. Therefore, it is expected that the W-O framework can electrocatalyze the reduction of 2,4-DNPH, while Cu ions can electrocatalyze the oxidation of the 2,4-DNPH metabolite; accordingly, $Cu_4P_4W_{30}$ was chosen to develop a two-way electrochemical sensor for the detection of 2,4-DNPH and its metabolite. Such a study has never been reported so far.

Graphene oxide (GO) is a two-dimensional carbon material with a hexagonal honeycomb crystal structure composed of a single layer of independent sp^2 hybrid carbon atoms [24]. Since GO was discovered in 2004, GO-based materials have attracted widespread attention and been applied in electronics, optics, catalysis, energy storage, electrochemical sensing, and other fields due to their excellent physical, chemical, optical, and electrical properties such as high conductivity, high carrier mobility, high specific surface area, and high catalytic activity [25–27]; moreover, GO-based materials have strong adsorption effects on functional components or organic pollutants, especially nitro aromatic compounds [28,29]. Therefore, in this work, GO was chosen as the component material for the construction of a composite film. However, the surface of both GO and $Cu_4P_4W_{30}$ are negatively charged; thus, they cannot be directly fabricated together due to the repulsive electrostatic interaction. Poly(diallyl dimethyl ammonium) (PDDA) is strong cationic polyelectrolyte and is easily soluble in water. Due to the rich positive charge and excellent conductivity, PDDA has been widely utilized as a support material to assemble composite films with a negatively charged component. To date, a series of POMs containing composite films have been fabricated using PDDA as the support material [30,31], which enables the functional features of POMs to be realized on the electrode surface. In addition, PDDA is a polyelectrolyte and is easily adsorbed on the surface of GO through electrostatic attraction to form the PDDA-GO complex with a positive charge, greatly increasing the assembly capacity of GO on the substrate surface [32]. In that study, the PDDA-GO complex was fabricated with $Cu_4P_4W_{30}$ via electrostatic attraction. One advantage is to increase the content of $Cu_4P_4W_{30}$ on the electrode surface. On the other hand, as is well known, apart

from the large surface area, GO has very good electrocatalytic activity. As shown in Figure S2, the GO-containing composite-film-modified electrode showed electrocatalytic activity for the reduction of 2,4-DNPH. Thus, another advantage is enhancing the electrocatalytic efficiency for the reduction of 2,4-DNPH through the synergistic effect between GO and $Cu_4P_4W_{30}$.

Layer-by-layer (LBL) self-assembly is a technology to grow composite films by alternating the deposition of oppositely charged substances on solid substrates, which allows the simple and stable control of the composite film structure at the nanoscale [33]. At present, the LBL deposition method is used in the preparation of GO-based films, capacitor organic films, luminescent films, and biofilms, as well as in other practical applications, such as to enhance the electrocatalytic activity of the electrode [34], in the electrochemical detection of methylparaben [35] and bisphenol A [36], and in energy storage and conversion [37].

In this work, on the ITO electrode, the composite film $(Cu_4P_4W_{30}/PDDA\text{-}GO)_n$ was constructed with the LBL method and the prepared electrode was then used as an electrochemical sensor to detect 2,4-DNPH and its metabolite.

For clarity, the structural formulas of 2,4-DNPH and PDDA are shown in Scheme 1.

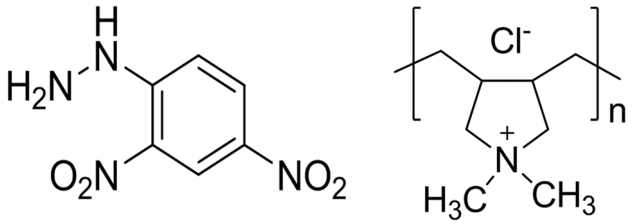

Scheme 1. The structural formulas of 2,4-DNPH (**a**) and PDDA (**b**).

2. Results and Discussion

2.1. Spectroscopic Characterization of $Cu_4P_4W_{30}$

Fourier-transform infrared spectroscopy (FT-IR) was used to characterize the structure of $Cu_4P_4W_{30}$, as shown in Figure 1a. It can be seen that the characteristic vibrating bands of $Cu_4P_4W_{30}$ appear at 1085 cm^{-1} for γ_{as} (P-O_a, O_a represents the oxygen atom in PO_4), 943 cm^{-1} for γ_{as} (W-O_d, O_d represents the terminal oxygen atom in MO_6 octahedra), 889 cm^{-1} for γ_{as} (W-O_b-W, O_b represents the oxygen atom for corner-sharing WO_6 octahedra), and 786 cm^{-1} for γ_{as} (W-O_c-W, O_c represents the oxygen atom for edge-sharing WO_6 octahedra), which are consistent with those reported in the literature [23], indicating that the compound $Cu_4P_4W_{30}$ was synthesized successfully. The UV-vis spectrum of $Cu_4P_4W_{30}$ is displayed in Figure 1b. It is obvious that $Cu_4P_4W_{30}$ has an absorption band at 267 nm, which is attributed to the characteristic absorption of POMs, corresponding to the charge transfer transition of $O_{b,c} \rightarrow W$ ($O_{2p} \rightarrow W_{5d}$).

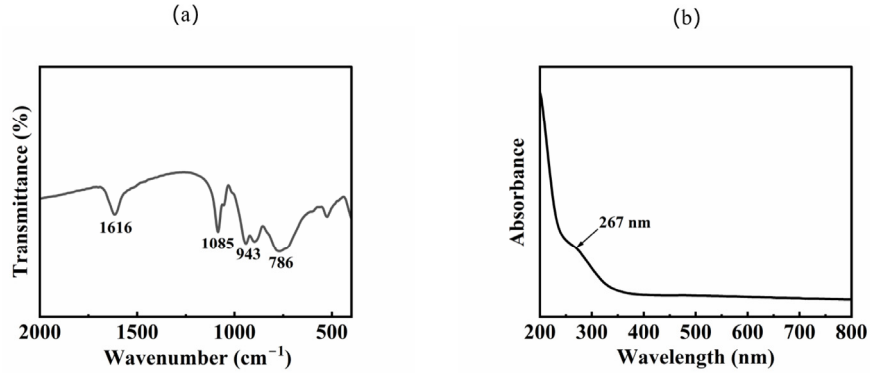

Figure 1. IR spectrum of $Cu_4P_4W_{30}$ (**a**) and UV-vis spectrum of 10^{-5} M $Cu_4P_4W_{30}$ (**b**).

2.2. Electrochemical Characterization of $Cu_4P_4W_{30}$ in Solution and on the Composite Film

Using cyclic voltammetry, the electrochemical behavior of the compound $Cu_4P_4W_{30}$ in solution was investigated. As shown in Figure 2a, the redox peaks of Cu and W are clearly observable at 0.051V/−0.29V (I/I′) for Cu and −0.462V/−0.667V (II/II′), −0.724V/−0.886V (III/III′) for W, which are consistent with those reported in the literature [22]

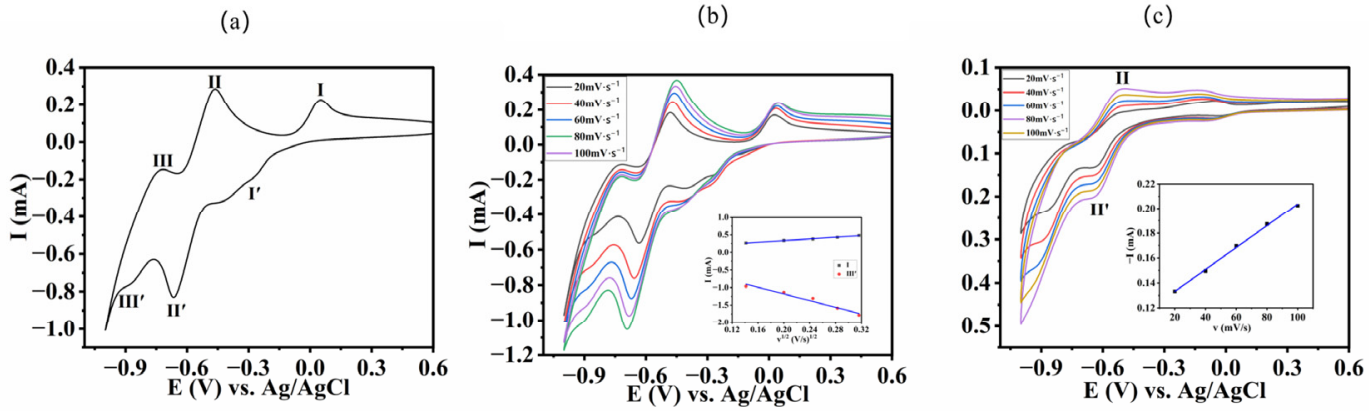

Figure 2. CV curve of bare ITO in 1.0 mM $Cu_4P_4W_{30}$ solution in 0.5 M HAc + 0.5 M NaAc at pH 5 with scan rate of 50 $mV{\cdot}s^{-1}$ (**a**); CV curves of $Cu_4P_4W_{30}$ in solution in 0.5 M HAc + 0.5 M NaAc (pH 5) at different scan rates from 20 to 100 $mV{\cdot}s^{-1}$; the inset shows the linear relationship between peak currents (II and II′) and square root of scan rates (**b**); CV curves of the ITO/$(Cu_4P_4W_{30}$/PDDA-GO$)_1$ electrode in 0.5 M HAc + 0.5 M NaAc (pH = 5) at different scan rates from 20 to 100 $mV{\cdot}s^{-1}$; the inset shows the linear relationship between the peak currents (II′) and scan rates (**c**).

The CVs of bare ITO in the $Cu_4P_4W_{30}$ solution at different scan rates of 20 to 100 $mV{\cdot}s^{-1}$ are shown in Figure 2b, giving a good linear relationship between the peak currents (II and II′) and the square root of the scan rates, confirming that the redox of $Cu_4P_4W_{30}$ in the solution is a diffusion-controlled electrochemical process. For comparison, the electrochemical behavior of the single layer of the film on the ITO/$(Cu_4P_4W_{30}$/PDDA-GO$)_1$ electrode at different scan rates from 20 to 100 $mV{\cdot}s^{-1}$ is shown in Figure 2c, and a good linear relationship between the redox peak currents (II′) and the scan rates is observable in the inset in Figure 2c, indicating that the redox process of the component $Cu_4P_4W_{30}$ on the ITO/$(Cu_4P_4W_{30}$/PDDA-GO$)_1$ electrode is a surface-controlled electrochemical reaction. Obviously, the different redox behaviors of $Cu_4P_4W_{30}$ in the solution and on the film proved that $Cu_4P_4W_{30}$ was adsorbed on the electrode surface and the redox property of $Cu_4P_4W_{30}$ was maintained very well on the film.

2.3. Film Characterization Containing $Cu_4P_4W_{30}$

2.3.1. UV-Vis Spectra Characterization

Using UV-vis absorption spectroscopy, the growth of the films containing $Cu_4P_4W_{30}$ and PDDA-GO on a quartz sheet was monitored. The assembly layer of PDDA-GO and $Cu_4P_4W_{30}$ was considered as one layer because $Cu_4P_4W_{30}$ has a negative charge and PDDA-GO possesses a positive charge. PDDA-GO helps $Cu_4P_4W_{30}$ to be deposited on the electrode surface. Therefore, the UV-vis spectrum of each assembly layer ($Cu_4P_4W_{30}$/PDDA-GO) was recorded. The UV-vis spectra of the films ($Cu_4P_4W_{30}$/PDDA-GO$)_{1–8}$ on the quartz sheet are shown in Figure 3a. It can be seen that the absorbance of the characteristic band of $Cu_4P_4W_{30}$ increased with the number of layers, demonstrating that the film of ($Cu_4P_4W_{30}$/PDDA-GO$)_{1–8}$ grew almost uniformly on the substrate.

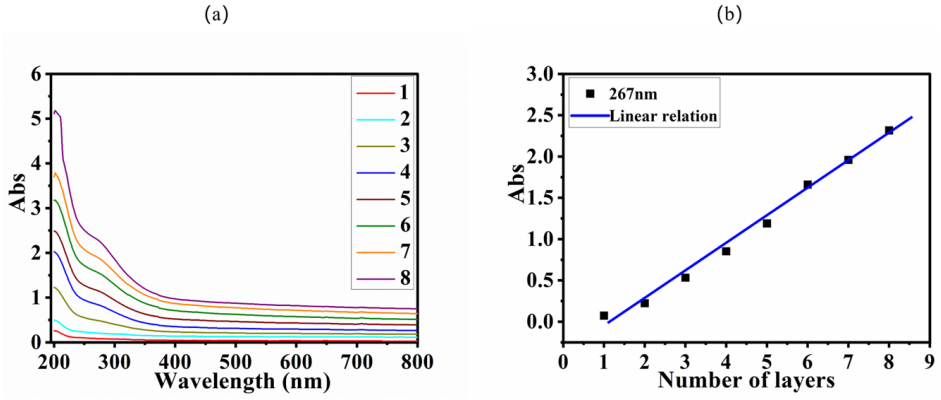

Figure 3. UV-vis spectra of the film $(Cu_4P_4W_{30}/PDDA\text{-}GO)_{1–8}$ on quartz sheet (**a**) and the relationship between the absorbance of the characteristic absorption bands at 267 nm and the layer number of the film (**b**). The black square corresponds the absorbance per layer number and the blue line corresponds the fitted linear relationship.

Compared with Figure 1b, the characteristic absorption band of $Cu_4P_4W_{30}$ in Figure 3a did not change significantly during the process of assembling the film, suggesting that the electronic structure of $Cu_4P_4W_{30}$ remained on the film. In addition, the UV-vis spectrum of PDDA-GO is shown in Figure S3. It can be seen that PDDA-GO displayed the absorption band at 230 nm and 300 nm. Comparing the UV-vis spectra of the composite films $(Cu_4P_4W_{30}/PDDA\text{-}GO)_{1–8}$ shown in Figure 3a with the UV-vis spectra of PDDA-GO and $Cu_4P_4W_{30}$ in the solution, it can be seen that the absorption bands at ca. 200 nm and 267 nm of the composite films $(Cu_4P_4W_{30}/PDDA\text{-}GO)_{1–8}$ mainly arose from $Cu_4P_4W_{30}$, while PDDA-GO did not show a significant influence in the studied wavelength region due to the small amount of PDDA-GO on the composite film.

2.3.2. Electrochemical Characterization

Furthermore, cyclic voltammetry was utilized to characterize the growth of the film. The CV curves of the ITO/$(Cu_4P_4W_{30}/PDDA\text{-}GO)_{3–8}$ electrode in the buffer solution were recorded, as shown in Figure 4a. It can be seen that in the blank buffer solution, the redox peak currents of the film-modified electrode increased with the increase in the number of layers, and there was a good linear relationship between the reduction peaks and the layer numbers (see Figure 4b), further confirming that the film of $(Cu_4P_4W_{30}/PDDA\text{-}GO)_{3–8}$ was deposited on the ITO electrode uniformly. This observation is consistent with that in the UV-vis spectra.

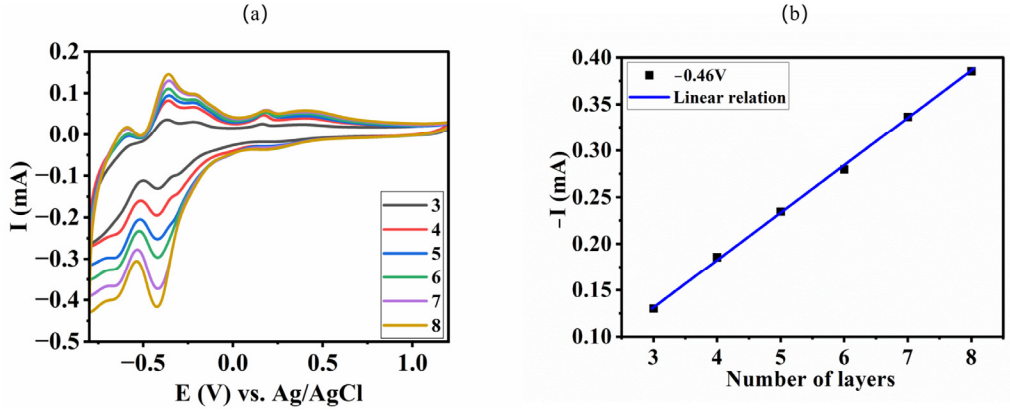

Figure 4. CV curves of the ITO/$(Cu_4P_4W_{30}/PDDA\text{-}GO)_{3–8}$ electrode in buffer solution at pH = 3 with scan rate of 50 $mV{\cdot}s^{-1}$ (**a**) and the linear relationship between the peak currents at −0.43 V and the layer number (**b**). The black square corresponds the current per layer number and the blue line corresponds the fitted linear relationship.

2.3.3. Effective Surface Area Evaluation of the Film-Modified Electrode

Using the LBL method, the film $(Cu_4P_4W_{30}/PDDA\text{-}GO)_6$ was fabricated on the surface of the ITO electrode to form the film-modified electrode. A series of CV curves at different scan rates from 20 to 100 $mV{\cdot}s^{-1}$ were measured using cyclic voltammetry in 1.0 mM $[Fe(CN)_6]^{3-/4-}$ mixed solution containing 0.1 M KCl (see Figure 5). Based on the Randles–Sevcik Equation (1), the A_{eff} of the modified electrode was calculated from the relationship between I_p and $v^{1/2}$ in the inset of Figure 5, giving 2.09 cm^2 for the ITO/$(Cu_4P_4W_{30}/PDDA\text{-}GO)_6$ electrode. Comparing it with the geometric area of the bare ITO electrode immersed in the solution (1.2 cm^2) indicates that the electrochemical active area of the ITO electrode increased after the modification of the film $(Cu_4P_4W_{30}/PDDA\text{-}GO)_6$.

$$I_p = 2.69 \times 10^5 \times n^{3/2} \times A_{eff} \times D^{1/2} \times c \times v^{1/2} \quad (1)$$

where I_p refers to the peak current, A is the electrode area (cm^2), c is the concentration of $[Fe(CN)_6]^{3-/4-}$, and v is the scan rate. For 1.0 mM $[Fe(CN)_6]^{3-/4-}$, n = 1, D = 7.6×10^{-6} $cm^2\ s^{-1}$ (0.1 M KCl) [38].

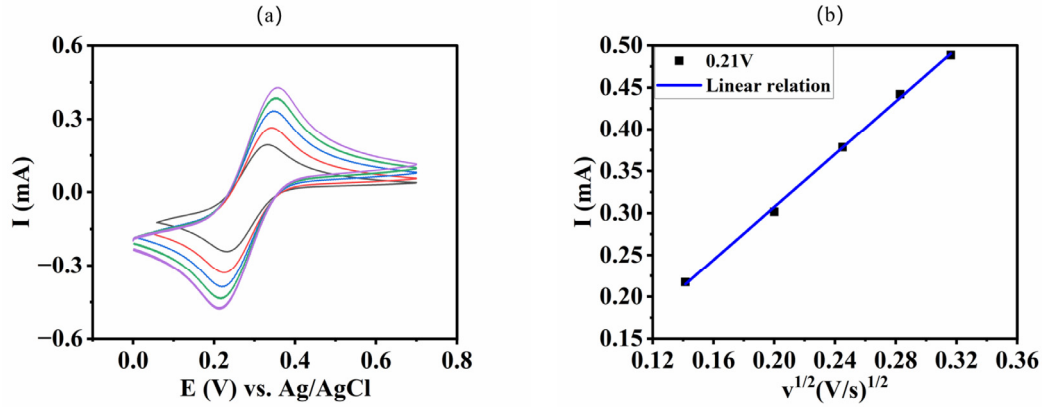

Figure 5. CVs of ITO/$(Cu_4P_4W_{30}/PDDA\text{-}GO)_6$ in 1.0 mM $[Fe(CN)_6]^{3-/4-}$ solution containing 0.1 M KCl at different scan rates (20, 40, 60, 80, and 100 $mV{\cdot}s^{-1}$) (**a**) and the linear relationship between the oxidation peak currents and the square root of scan rates (**b**).The black square corresponds the current per square root of scan rates and the blue line corresponds the fitted linear relationship.

2.4. Electrocatalytic Activity of the ITO/$(Cu_4P_4W_{30}/PDDA\text{-}GO)_6$ Electrode for the Reduction of 2,4-DNPH

2.4.1. Electrocatalytic Activity of Bare ITO Electrode for the Reduction of 2,4-DNPH

First, the CVs of bare ITO in different concentrations of 2,4-DNPH were recorded, as shown in Figure 6a; it can be seen that in the potential range of −1.0 V to 1.0 V, the currents of the reduction peaks at −1.0 V increased with the increase in 2,4-DNPH concentrations, but no obvious oxidation peaks were observed in the positive potential range from 0 to 1.0 V, indicating 2,4-DNPH can be electrochemically reduced at the bare ITO electrode at −1.0 V, but its metabolite cannot be oxidized at the bare ITO. Second, the CVs of the bare ITO in the blank solution, $Cu_4P_4W_{30}$ solution (1.0 mM), 2,4-DNPH solution (10 μM) and the mixed solution of $Cu_4P_4W_{30}$ (1.0 mM) and 2,4-DNPH (10 μM) were compared, as shown in Figure 6b; it is clearly noted that the reduction peak current of the W-O framework at −0.70 V increased, while the oxidation peak current of Cu at +0.06 V increase after adding 2,4-DNPH, clearly demonstrating the W-O framework catalyzed the reduction of 2,4-DNPH and Cu^{2+} catalyzed the oxidation of the 2,4-DNPH metabolite.

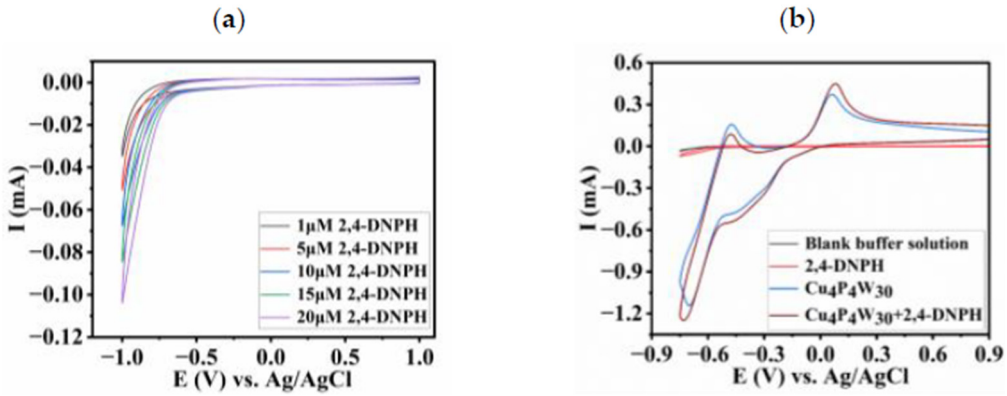

Figure 6. CVs of bare ITO in 2,4-DNPH at different concentrations (pH 7) with scan rate of 50 mV·s^{-1} (**a**) and CVs of bare ITO in different solutions (pH 7) with scan rate of 50 mV·s^{-1} (**b**).

2.4.2. Electrocatalytic Activity of the ITO/$(Cu_4P_4W_{30}$/PDDA-GO$)_6$ Electrode for the Reduction of 2,4-DNPH

In order to confirm the observation above, the film-modified ITO/$(Cu_4P_4W_{30}$/PDDA-GO$)_6$ electrode was constructed and the electrocatalytic activity was investigated. As shown in Figure 7, it can be clearly observed that the ITO/$(Cu_4P_4W_{30}$/PDDA-GO$)_6$ electrode showed obvious electrocatalytic activity for the reduction of 2,4-DNPH and the oxidation of the 2,4-DNPH metabolite; apparently, the reduction peak current of the W-O framework and the oxidation peak current of Cu increased after adding 2,4-DNPH (10 μm). This observation is consistent with the case in the solution, indicating the electrocatalytic activity of $Cu_4P_4W_{30}$ remained on the film. Taking the peak current at the concentration of 10 μm 2,4-DNPH as the example, the value of catalytic efficiency (CAT) was calculated to be 90.2% at −0.542 V for the reduction of 2,4-DNPH and 191.6% at 0.27 V for the oxidation of the 2,4-DNPH metabolite, according to the following Equation (2) [39]. These results definitely confirm that the constructed ITO/$(Cu_4P_4W_{30}$/PDDA-GO$)_6$ electrode could be employed as a two-way electrochemical sensor to detect 2,4-DNPH and its metabolite.

$$\text{CAT} = 100\% \times [I_p \text{ (modified electrode in 2,4-DNPH solution)} - I_p \text{ (modified electrode in blank solution)}]/I_p \text{ (modified electrode in blank solution)} \quad (2)$$

where I_p represents the reduction peak current in the presence and absence of 2,4-DNPH, respectively.

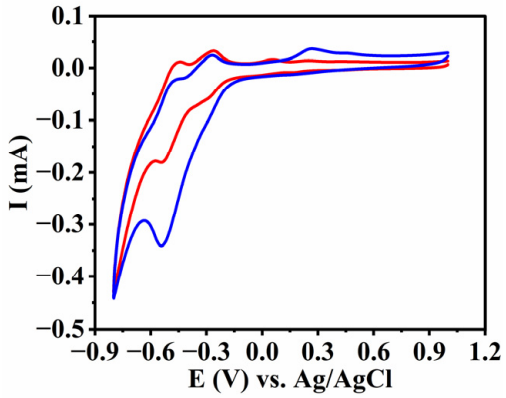

Figure 7. CV curves of the ITO/$(Cu_4P_4W_{30}$/PDDA-GO$)_6$ electrode in blank buffer solution (red curve) and 2,4-DNPH solution (10 μm, blue curve) at pH 3 with scan rate of 50 mV·s^{-1}.

2.4.3. Effect of the Layer Number of the Film $(Cu_4P_4W_{30}/PDDA\text{-}GO)_n$ on the Electrocatalytic Activity for the Reduction of 2,4-DNPH

The effect of the layer number on electrocatalytic performance was investigated. For this purpose, a series of comparative experiments were carried out on the film $(Cu_4P_4W_{30}/PDDA\text{-}GO)_n$ (n = 3–8)-modified electrode to find the optimal number of layers for the electrocatalytic reduction of 2,4-DNPH. It can be observed that as shown in Figure 8, the reduction currents of 10 μM 2,4-DNPH increased with the increase in the number of layers until the number of layers (n) was 7, while it decreased when n was 8. The possible reason for this observation is that the thickness of the film increases with the number of layers, while the electron exchange path from the film surface to the electrode surface becomes longer, which leads to the difficulty of electron transfer. Therefore, the optimal number of layers of the film-modified electrode is considered to be seven for the following sensing performance study.

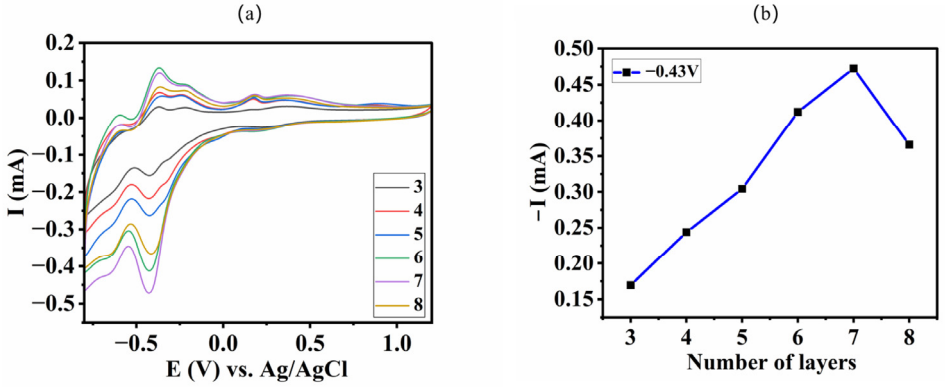

Figure 8. CV curves of the ITO/$(Cu_4P_4W_{30}/PDDA\text{-}GO)_n$ electrode (n = 3, 4, 5, 6, 7, and 8) in 10 μm 2,4-DNPH at pH 3 (**a**) and the relationship between the reduction currents at −0.43 V and the layer number (**b**), scan rate: 50 $mV{\cdot}s^{-1}$.

2.5. Effect of pH Value on the Reduction Peak Potential of 2,4-DNPH

The effect of solution pH on the reduction peak potential of 2,4-DNPH was investigated in buffer solution containing 10 μM 2,4-DNPH at different pH values from 1 to 8. As shown in Figure 9, with the increase in the solution pH value, the potentials of the reduction peak of 2,4-DNPH moved to the negative direction, indicating the reduction of 2,4-DNPH was accompanied by proton involvement. The relationship between the pH values and the reduction peak potentials was obtained as $E = -0.065\ pH - 0.3427$ ($R^2 = 0.988$). It can be seen that the slope of 0.065 V/pH is close to the theoretical value of 0.059(m/n) V per pH based on the Nernst equation, in which m expresses the number of protons transferred and n represents the number of electrons participating in the electron transfer reaction. The value of m/n was calculated to be 1.1, indicating an electron transfer process involving equal numbers of protons and electrons. This observation is consistent with a report in the literature [1], where the authors demonstrated that 2,4-DNPH can be electrochemically reduced to 2,4-diamino-phenylhydrazine by six electrons and six protons participating in each nitro group. Then, the 2,4-DNPH metabolite was further oxidized to 2,4-diamino-phenylhydrazone, catalyzed by Cu^{2+} [40].

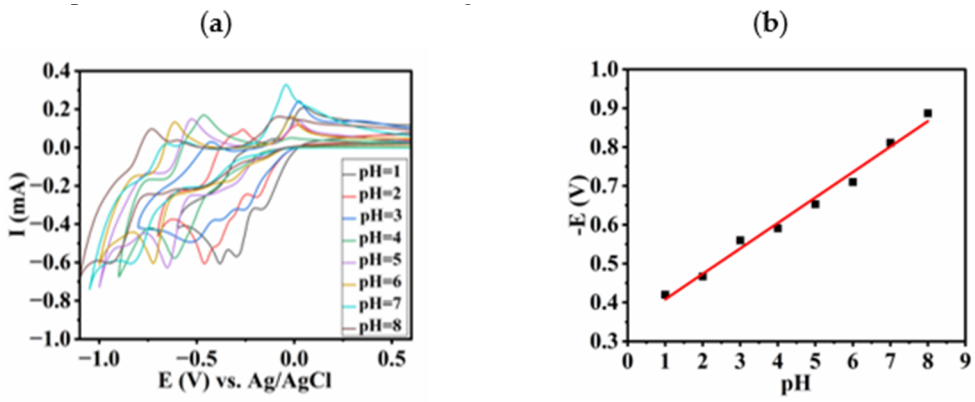

Figure 9. CVs of the ITO/$(Cu_4P_4W_{30}$/PDDA-GO$)_7$ electrode in different pH solutions from 1 to 8 containing 10 μm 2,4-DNPH with scan rate: 50 mV·s^{-1} (**a**) and the relationship of reduction potentials and the solution pHs (**b**).

Additionally, it can be seen from Figure 9a that in different pH solutions, the reduction peak currents of 2,4-DNPH at the ITO/$(Cu_4P_4W_{30}$/PDDA-GO$)_7$ electrode did not display significant changes. This observation suggests that the prepared ITO/$(Cu_4P_4W_{30}$/PDDA-GO$)_7$ electrode can be utilized to detect 2,4-DNPH in a wide pH range. Considering environmental protection and that most real samples are in neutral conditions, pH 7 was elected for the following work.

2.6. Sensing Performance of the ITO/$(Cu_4P_4W_{30}$/PDDA-GO$)_7$ Electrode

Figure 10 depicts the CV curves of the ITO/$(Cu_4P_4W_{30}$/PDDA-GO$)_7$ electrode in different concentrations of 2,4-DNPH (1–40 μm) in the potential range from −0.9 to 1.0 V. It can be clearly seen that the response currents gradually increased with the increase in the concentration of 2,4-DNPH. For clarity, the CVs in the potential range from 0 to −0.9 V and from 0 to 1.0 V are separately shown in Figure 10b,d, while the calibration curves for the detection of 2,4-DNPH and its metabolite are plotted in Figure 10c,e, which show different linear relationships between the catalytic currents and the concentrations of 2,4-DNPH. When the concentration range of 2,4-DNPH changed from 1 to 40 μm, the linear correlations were I (μA) = −30.2 c (μM) − 222 (R^2 = 0.994) for the detection of 2,4-DNPH and I (μA) = 6.88 c (μM) + 36.25 (R^2 = 0.992) for the detection of the 2,4-DNPH metabolite, respectively. Furthermore, the limit of detection (LOD) [41] of the prepared sensor ITO/$(Cu_4P_4W_{30}$/PDDA-GO$)_7$ was calculated to be 35.6 nM for the detection of 2,4-DNPH based on signal-to-noise ratio 3 (S/N = 3). Then, the obtained result was compared with reported LOD values obtained using other detection methods in the literature; it can be seen from Table 1 that the developed sensor achieved a good sensing performance. Moreover, the proposed sensor was simply prepared at a low cost and showed a two-way electrochemical sensing performance for the detection of 2,4-DNPH and its metabolite.

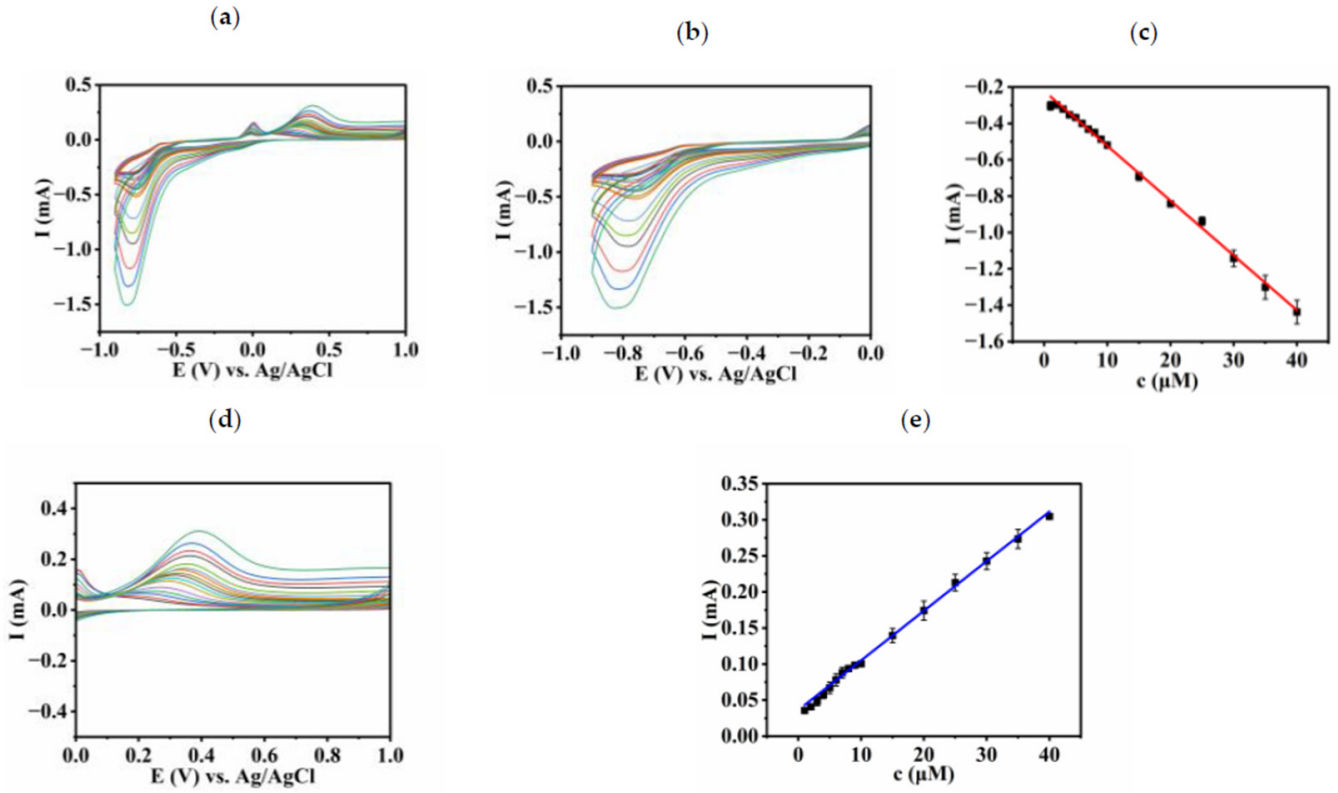

Figure 10. CVs of the ITO/$(Cu_4P_4W_{30}$/PDDA-GO$)_7$ electrode in different concentrations of 2,4-DNPH (1–40 μm) (**a**); CVs in the potential range from 0 to −0.9 V (**b**) and the linear relationship between reduction peak currents and concentration of 2,4-DNPH (1–40 μm) (**c**); CVs in the range from 0 to 1.0 V (**d**) and the linear relationship between the oxidation peak currents and concentration of 2,4-DNPH (1–40 μm) (**e**) at pH 7.0 with scan rate of 50 mV·s^{-1}.

Table 1. Comparison of different materials for 2,4-DNPH detection.

Material	Electrode	Technique	LOD (nM)	Linear Range (μM)	Reference
P-pABA-MnO_2	GCE	LSV	80	0.5–90	[1]
Zn-MOF	-	Fluorescence	100	0.1–500	[11]
Cu^{II} ions	GCE	CA	5.5	0.01–10	[15]
$(P_8W_{48}$/PDDA$)_7$	ITO	CV	12	1.0–700	[16]
Cu^{II} ions	GCE	EIS	40	0.01–100	[40]
$(Cu_4P_4W_{30}$/PDDA-GO$)_7$	ITO	CV	35.6	1.0–40	This work

2.7. Stability, Reproducibility, and Repeatability Evaluation of the Film-Modified Electrodes

Stability, reproducibility, and repeatability are very important indexes to evaluate the performance of electrochemical sensors in the sensing process. To determine whether the sensor response of the ITO/$(Cu_4P_4W_{30}$/PDDA-GO$)_7$ electrode to 2,4-DNPH was reproducible, seven consecutive readings were taken in 10 μM 2,4-DNPH at pH 7 using the same electrode. As shown in Figure 11a, the results indicate that the relative standard deviation (RSD) of the peak currents was 1.23% for the reduction peak at −0.88 V and 2.60% for the oxidation peak at 0.36 V, meaning that the sensor prepared for the detection of 2,4-DNPH had good reproducibility. Furthermore, the repeatability of the ITO/$(Cu_4P_4W_{30}$/PDDA-GO$)_7$ electrode was evaluated using five different electrodes prepared within five days, and their response currents to 10 μM 2,4-DNPH at pH 7 was recorded (shown in Figure 11b), giving RSDs of 2.45% for the reduction peak at −0.88V and 3.01% for the oxidation peak at 0.36 V, implying that the ITO/$(Cu_4P_4W_{30}$/PDDA-GO$)_7$ electrode had good repeatability. Finally, the operational stability of the ITO/$(Cu_4P_4W_{30}$/PDDA-GO$)_7$ electrode was tested

by scanning 100 cycles continuously in 10 μM 2,4-DNPH at pH 7; the corresponding CVs are shown Figure 10c, showing that the peak current remained at about 90.9% of the initial value after scanning 100 cycles, which proves that the ITO/$(Cu_4P_4W_{30}$/PDDA-GO)$_7$ electrode possessed good stability. Based on the above observation, it can be concluded that the proposed ITO/$(Cu_4P_4W_{30}$/PDDA-GO)$_7$ electrode could be used as a stable, reproducible, and repeatable electrochemical sensor for the detection of 2,4-DNPH and its metabolite.

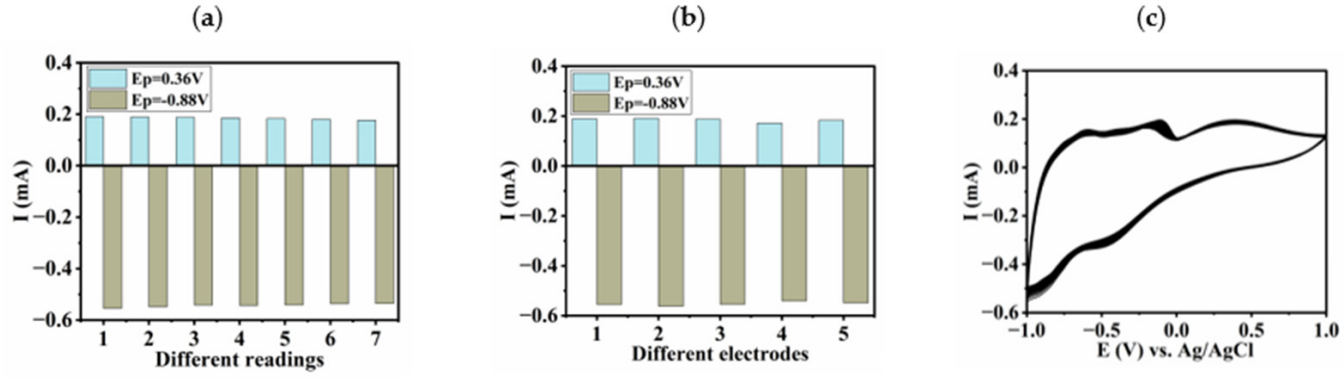

Figure 11. The current value of the ITO/$(Cu_4P_4W_{30}$/PDDA-GO)$_7$ electrode continuously recorded 7 times in 10 μm 2,4-DNPH solution at E_p = −0.88 V and 0.36 V (**a**); the recorded current values of five ITO/$(Cu_4P_4W_{30}$/PDDA-GO)$_7$ electrodes prepared in different days in 10 μm 2,4-DNPH solution at E_p = −0.88 V and 0.36 V (**b**); CVs of the ITO/$(Cu_4P_4W_{30}$/PDDA-GO)$_7$ electrode in 10 μM 2,4-DNPH scanned continuously for 100 times at pH 7.0 at a scan rate of 50 mV·s^{-1} (**c**).

3. Materials and Method

3.1. Materials

$Cu_4P_4W_{30}$ was synthesized according to the procedure reported in the literature [23]; GO was prepared using the modified Hummers method proposed by Kovtyukhova and colleagues [42]. Poly (diallyl dimethyl ammonium chloride) (PDDA Mw = 100,000–200,000, 20 wt% in water) was purchased from Aldrich. PDDA-GO was formed based on the literature [32]. Buffer solutions were prepared with 0.5 M NaH_2PO_4 and 0.5 M Na_2HPO_4 (pH 7~8), 0.5 M HAc and 0.5 M NaAc (pH 4~6), and 0.5 M H_2SO_4 and 0.5 M Na_2SO_4/Li_2SO_4 (pH 1~3), respectively. The three-electrode system included a 3M KCl-filled Ag/AgCl reference electrode, a bare ITO (indium tin oxide) or modified ITO working electrode, and a platinum wire counter electrode.

3.2. Preparation of the Film-Modified Electrode

3.2.1. The Pretreatment of the Substrates

The substrates needed to be cleaned before use. In this work, the ITO electrode was used for the electrochemical study. The quartz sheet was utilized for the UV-vis spectra characterization of the film. The cleaning process of the two substrates was as follows:

The cleaning of the ITO electrode [43]: 1 M NaOH and ethanol were mixed with a volume ratio of 1:1 to form a cleaning solution. The ITO piece was placed in the cleaning solution for 10 min via sonication; then, it was rinsed repeatedly with deionized water and gently dried with nitrogen.

The cleaning of the quartz sheet [44]: Concentrated sulfuric acid and hydrogen peroxide were mixed at a volume ratio of 7:3 to form a cleaning solution. The quartz sheet was heated to 80 °C for 1 h in the cleaning solution; then, it was rinsed repeatedly with deionized water and gently dried with nitrogen.

3.2.2. Fabrication of the Film on the Substrates

The films [PDDA/$(Cu_4P_4W_{30}$/PDDA-GO)]$_n$ were fabricated using the LBL method based on the principle of electrostatic interaction. The specific steps are described as follows: Firstly, a PDDA solution with a mass fraction of 8 wt% was configured, and

the cleaned substrates were immersed in it and soaked for 10 h so that the surface of the substrates was assembled with positively charged PDDA. Then, the substrates were rinsed slowly with deionized water and dried slowly with nitrogen. Secondly, the PDDA-modified substrates were immersed in 1 mM $Cu_4P_4W_{30}$ and PDDA-GO solution (1 mg mL^{-1}) for 20 min alternately and repeatedly to construct the film $(Cu_4P_4W_{30}/PDDA\text{-}GO)_n$-modified substrates. The above operation process was repeated several times to fabricate the film $(Cu_4P_4W_{30}/PDDA\text{-}GO)_n$ with different layers. The assembly process is depicted in Scheme 2.

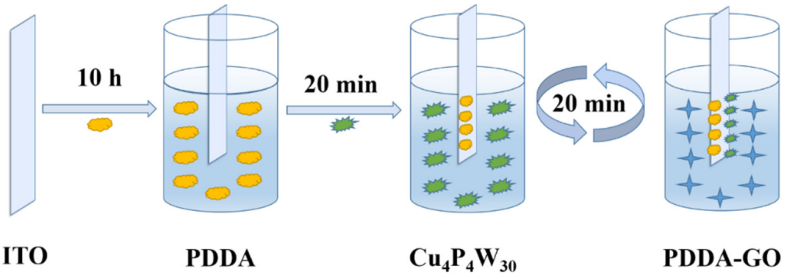

Scheme 2. Schematic diagram of preparation of the film $(Cu_4P_4W_{30}/PDDA\text{-}GO)_n$ on ITO. (Yellow symbol is PDDA, green symbol is $Cu_4P_4W_{30}$, and blue symbol is PDDA-GO.)

4. Conclusions

In this work, a novel two-way electrochemical sensor was successfully developed based on a functional-component-modified ITO electrode via the fabrication of PDDA-GO and $Cu_4P_4W_{30}$. The prepared modified electrode not only catalyzed the reduction of 2,4-DNPH to 2,4-diamino-phenylhydrazine arising from the catalysis of the W-O framework in $Cu_4P_4W_{30}$, but also catalyzed the oxidation of the 2,4-DNPH metabolite to 2,4-diamino-phenylhydrazone arising from the catalysis of the Cu cluster in $Cu_4P_4W_{30}$. The UV-vis spectra and CVs clearly demonstrated that the $Cu_4P_4W_{30}$ component was assembled on the surface of the ITO and its electrocatalytic activity was maintained on the ITO; thus, a new electrochemical sensor for sensing the response of 2,4-DNPH was successfully manufactured. The explored sensor showed a good LOD of 35.6 nM in the linear range from 1 to 40 μm based on S/N = 3. Moreover, further evaluation indicated the sensor possessed good stability, reproducibility, and repeatability. Therefore, it is anticipated that the proposed two-way electrochemical sensor could give important information on the removal of 2,4-DNPH from water to provide a clean water source.

Supplementary Materials: The following supporting information can be downloaded at: https://www.mdpi.com/article/10.3390/catal13040769/s1, Figure S1: The structure of $Cu_4P_4W_{30}$. Figure S2: CVs of bare ITO and the ITO/$[PDDA\text{-}GO/PSS]_7$ electrode in blank buffer solution and 2,4-DNPH solutions. Figure S3: UV-vis absorption spectrum of GO dispersion.

Author Contributions: Conceptualization. X.Y. (Xiaolei Yan), X.Y. (Xiaoxia Yu) and L.B.; validation, X.Y. (Xiaolei Yan), X.Y. (Xiaoxia Yu) and L.B.; formal analysis, X.Y. (Xiaolei Yan), X.Y. (Xiaoxia Yu) and L.B.; investigation, X.Y. (Xiaolei Yan), X.Y. (Xiaoxia Yu) and J.P.; resources, X.Y. (Xiaolei Yan), X.Y. (Xiaoxia Yu) and J.P.; data curation, X.Y. (Xiaolei Yan) and X.Y. (Xiaoxia Yu); writing—original draft preparation, X.Y. (Xiaolei Yan) and X.Y. (Xiaoxia Yu); writing—review and editing, X.Y. (Xiaolei Yan) and L.B.; visualization, X.Y. (Xiaolei Yan) and X.Y. (Xiaoxia Yu); supervision, L.B. All authors have read and agreed to the published version of the manuscript.

Funding: This research received no external funding.

Data Availability Statement: The data presented in this study are available on request from the corresponding author. The data are not publicly available due to the need for follow-up research.

Acknowledgments: We thank the co-authors for their help in writing this article, the reviewers for their comments and valuable opinions, and the editors for their help in publishing this article.

Conflicts of Interest: The authors declared no conflict of interest.

References

1. Adeosun, W.; Asiri, A.; Marwani, H. Real Time Detection and Monitoring of 2, 4-Dinitrophenylhydrazine in Industrial Effluents and Water Bodies by Electrochemical Approach Based on Novel Conductive Polymeric Composite. *Ecotoxicol. Environ. Saf.* **2020**, *206*, 111171. [CrossRef]
2. Li, J.; Joelle, E.; Yang, Q.; Zheng, F.; Liu, J. Determination of Residual Phenylhydrazines in Drug Substances by High-Performance Liquid Chromatography with Pre-column Derivatization. *Anal. Methods* **2019**, *11*, 6146–6152. [CrossRef]
3. Meng, Z.; Yin, J.; Zhao, F.; Li, M.; Zhang, Y.; Liang, Y.; Wang, Z.; Yang, Y. An Efficient Chitosan-Based Naphthalimide-Modified Fluorescent Sensor for Rapid Detection of 2,4-Dinitrophenylhydrazine and Its Applications in Environmental Analysis. *Eur. Polym. J.* **2021**, *158*, 110705. [CrossRef]
4. Malaei, R.; Ramezani, A.; Absalan, G. Analysis of Malondialdehyde in Human Plasma Samples Through Derivatization with 2,4-Dinitrophenylhydrazine by Ultrasound-Assisted Dispersive Liquid–Liquid Microextraction-GC-FID Approach. *J. Chromatogr. B* **2018**, *1089*, 60–69. [CrossRef] [PubMed]
5. Panchompoo, J.; Aldous, L.; Downing, C.; Crossley, A.; Compton, R. Facile Synthesis of Pd Nanoparticle Modified Carbon Black for Electroanalysis: Application to the Detection of Hydrazine. *Electroanalysis* **2011**, *23*, 1568–1578. [CrossRef]
6. Wang, Q.; Wang, X.; Wu, Y. Highly Sensitive and Selective Fluorescence Probe for 2,4-Dinitrophenylhydrazine Detection in Wastewater Using Water-Soluble CdTe QDs. *Photochem. Photobiol.* **2019**, *95*, 895–900. [CrossRef]
7. Chiş, V.; Filip, S.; Miclăuş, V.; Pîrnău, A.; Tănăselia, C.; Almăşan, V.; Vasilescu, M. Vibrational Spectroscopy and Theoretical Studies on 2,4-Dinitrophenylhydrazine. *J. Mol. Struc.* **2005**, *744–747*, 363–368. [CrossRef]
8. Yilmaz, B.; Asci, A.; Kucukoglu, K.; Albayrak, M. Simple High-Performance Liquid Chromatography Method for Formaldehyde Determination in Human Tissue through Derivatization with 2,4-Dinitrophenylhydrazine. *J. Sep. Sci.* **2016**, *39*, 2963–2969. [CrossRef]
9. Boumya, W.; Hammani, H.; Laghrib, F.; Lahrich, S.; Farahi, A.; Achak, M.; Bakasse, M.; Mhammedi, M.A.E. Electrochemical Study of 2,4-Dinitrophenylhydrazine as Derivatization Reagent and Aldehydes at Carbon Glassy Electrode. *Electroanalysis* **2017**, *29*, 1700–1711. [CrossRef]
10. Boumya, W.; Achak, M.; Bakasse, M.; el Mhammedi, M. Indirect Determination of Dopamine and Paracetamol by Electrochemical Impedance Spectroscopy Using Azo Coupling Reaction with Oxidized 2,4-Dinitrophenylhydrazine (DNPH): Application in Commercial Tablets. *J. Sci. Adv. Mater. Dev.* **2020**, *5*, 218–223. [CrossRef]
11. Zhang, E.; Ju, P.; Zhang, Z.; Yang, H.; Tang, L.; Hou, X.; You, J.; Wang, J. jiang A Novel Multi-Purpose Zn-MOF Fluorescent Sensor for 2,4-Dinitrophenylhydrazine, Picric Acid, La^{3+} and Ca^{2+}: Synthesis, Structure, Selectivity, Sensitivity and Recyclability. *Spectrochim. Acta A Mol. Biomol. Spectrosc.* **2019**, *222*, 117207. [CrossRef] [PubMed]
12. Singha, J.; Samanta, T.; Shunmugam, R. Unusual Redshift Due to Selective Hydrogen Bonding between F-Ion and Sensor Motif: A Naked Eye Colorimetric Sensor for F-Ions in an Aqueous Environment. *Mater. Adv.* **2020**, *1*, 2346–2356. [CrossRef]
13. Hassoni, F.; Mashkour, M. Spectrophotometric Determination of Anti-Ulcer Drug (Cimetidine) By 2.4-Dinitrophenylhydrazine Reagent. *J. Pharm. Negat. Results* **2022**, *13*, 192–199. [CrossRef]
14. Wang, Y.; Yang, X.; Bai, J.; Jiang, X.; Fan, G. High Sensitivity Hydrogen Peroxide and Hydrazine Sensor Based on Silver Nanocubes with Rich {100} Facets as an Enhanced Electrochemical Sensing Platform. *Biosens. Bioelectron.* **2013**, *43*, 180–185. [CrossRef]
15. Boumya, W.; Hammani, H.; Loudiki, A.; Achak, M.; Aboulkas, A.; Bakasse, M.; el Mhammedi, M. Use of the Oxidizing Effect of Copper (II) to Determine 2,4-Dinitrophenylhydrazine at Glassy Electrode by Chronoamperometry. *J. Electroanal. Chem.* **2015**, *759*, 77–81. [CrossRef]
16. Yu, X.; Pei, J.; Bi, L. Electrochemical Sensor Based on Polyoxometalate immobilized Using Layer-by-Layer Assembly Process to Detect 2,4-Dinitrophenylhydrazine. *New. J. Chem.* **2022**, *46*, 10777–10786. [CrossRef]
17. Liu, J.; Zhao, J.; Streb, C.; Song, Y. Recent advances on high-nuclear polyoxometalate clusters. *Coord. Chem. Rev.* **2022**, *471*, 214734. [CrossRef]
18. Ke, D.; Huang, S.; Yang, G. Lanthanide-Anderson Polyoxometalates Frameworks: Efficient Sulfide Photooxidation. *Inorg. Chem.* **2022**, *61*, 20080–20086. [CrossRef]
19. Li, B.; Xuan, L.; Wu, L. Polyoxometalate-Containing Supramolecular Gels. *Macromol. Rapid Commun.* **2022**, *43*, 2200019. [CrossRef]
20. Wu, Y.; Yu, X.; Fu, Z.; Pei, J.; Bi, L. Fabrication of Six Manganese Containing Polyoxometalate Modified Graphite C_3N_4 Nanosheets Catalysts Used to Catalyze Water Decomposition. *Catalysts* **2021**, *11*, 856. [CrossRef]
21. Pei, J.; Bi, L. Application of Composite Film Containing Polyoxometalate Ni25 and Reduced Graphene Oxide for Photoelectrocatalytic Water Oxidation. *Catalysts* **2022**, *12*, 696. [CrossRef]
22. Keita, B.; Mbomekalle, I.; Nadjo, L. Redox Behaviours and Electrocatalytic Properties of Copper within Dawson Structure-Derived Sandwich Heteropolyanions $[Cu_4(H_2O)_2(X_2W_{15}O_{56})_2]^{16-}$ (X = P or As). *Electrochem. Commun.* **2003**, *5*, 830–837. [CrossRef]
23. Kinke, R.; Droege, M.; Domaille, P. Trivacant Heteropolytungstate Derivatives. Rational Syntheses, Characterization, Two-Dimensional Tungsten-183 NMR, and Properties of Tungstometallophosphates $P_2W_{18}M_4(H_2O)_2O_{68}^{10-}$ and $P_4W_{30}M_4(H_2O)_2O_{112}^{16-}$ (M = cobalt, copper, zinc). *Inorg. Chem.* **1987**, *26*, 3886–3896. [CrossRef]
24. Inagaki, M.; Kang, F. Graphene Derivatives: Graphane, Fluorographene, Graphene Oxide, Graphyne and Graphdiyne. *J. Mater. Chem. A Mater.* **2014**, *2*, 13193–13206. [CrossRef]
25. Sattar, T. Current Review on Synthesis, Composites and Multifunctional Properties of Graphene. *Top. Curr. Chem.* **2019**, *377*, 10. [CrossRef]

26. Monajjemi, M. Metal-Doped Graphene Layers Composed with Boron Nitride–Graphene as an Insulator: A Nano-Capacitor. *J. Mol. Model.* **2014**, *20*, 1–8. [CrossRef]
27. Deka, M.; Baruah, U.; Chowdhury, D. Insight into Electrical Conductivity of Graphene and Functionalized Graphene: Role of Lateral Dimension of Graphene Sheet. *Mater. Chem. Phys.* **2015**, *163*, 236–244. [CrossRef]
28. Hong, X.; Wang, X.; Li, Y.; Fu, J.; Liang, B. Progress in Graphene/Metal Oxide Composite Photocatalysts for Degradation of Organic Pollutants. *Ctalysts* **2020**, *10*, 921. [CrossRef]
29. Baig, N.; Ihsanullah; Sajid, M.; Saleh, T. Graphene-Based Adsorbents for the Removal of Toxic Organic Pollutants: A Review. *J. Environ. Manag.* **2019**, *244*, 370–382. [CrossRef]
30. Gao, W.; Zheng, D.; Dong, Z.; Wu, L.; Bi, L. Preparation of Green Luminescence Composite Film and Study of Electrofluorochromic Performance. *J. Electroanal. Chem.* **2015**, *756*, 30–35. [CrossRef]
31. Ensafi, A.; Heydari-Soureshjani, E.; Jafari-Asl, M.; Rezaei, B. Polyoxometalate-Decorated Graphene Nanosheets and Carbon Nanotubes, Powerful Electrocatalysts for Hydrogen Evolution Reaction. *Carbon* **2016**, *99*, 398–406. [CrossRef]
32. Zhang, L.; Li, S.; Zhang, Z.; Tan, L.; Pang, H.; Ma, H. Facile Fabrication of Reduced Graphene Oxide and Keggin-Type Polyoxometalates Nanocomposite Film for High Performance Electrocatalytic Oxidation of Nitrite. *J. Electroanal. Chem.* **2017**, *807*, 97–103. [CrossRef]
33. Xu, L.; Zhang, H.; Feng, L.; Li, X.; An, Q. A Scalable Interfacial Engineering Strategy for a Finely Tunable, Homogeneous MoS_2/rGO-Based HER Catalytic Structure. *Adv. Mater. Interfaces* **2020**, *7*, 1902022. [CrossRef]
34. Ribicki, A.; Chemin, B.; van Haandel, V.; Winiarski, J.; de Castro Rozada, T.; Pessoa, C.; Estrada, R.; Fiorin, B.; Fujiwara, S. Sol Gel Synthesis of 3-n-Propyl(4-Aminomethyl)Pyridinium Silsesquioxane Chloride and the Enhanced Electrocatalytic Activity of LbL Films. *J. Solgel Sci. Technol.* **2018**, *87*, 216–229. [CrossRef]
35. de Lima, L.; Daikuzono, C.; Miyazaki, C.; Pereira, E.; Ferreira, M. Layer-by-Layer Nanostructured Films of Magnetite Nanoparticles and Polypyrrole towards Synergistic Effect on Methylparaben Electrochemical Detection. *Appl. Surf. Sci.* **2020**, *505*, 144278. [CrossRef]
36. Almeida, L.; Rodrigues, B.; Balogh, D.; Sanfelice, R.; Mercante, L.; Frade-Barros, A.; Pavinatto, A. Chitosan/Gold Nanoparticles Nanocomposite Film for Bisphenol A Electrochemical Sensing. *Electrochem* **2022**, *3*, 239–247. [CrossRef]
37. Guzmán, E.; Ortega, F.; Rubio, R. Layer-by-Layer Materials for the Fabrication of Devices with Electrochemical Applications. *Energies* **2022**, *15*, 3399. [CrossRef]
38. Yokus, O.; Kardas, F.; Akyildirim, O.; Eren, T.; Atar, N.; Yola, M. Sensitive Voltammetric Sensor Based on Polyoxometalate/reduced Graphene Oxide Nanomaterial: Application to the Simultaneous Determination of L-Tyrosine and L-Tryptophan. *Sensor. Actuat. B-Chem.* **2016**, *233*, 47–54. [CrossRef]
39. Jiao, J.; Zuo, J.W.; Pang, H.J.; Tan, L.C.; Chen, T.; Ma, H.Y. A dopamine electrochemical sensor based on Pd-Pt alloy nanoparticles decorated polyoxometalate and multiwalled carbon nanotubes. *J. Electroanal. Chem.* **2018**, *827*, 103–111. [CrossRef]
40. Boumya, W.; Hammani, H.; Loudiki, A.; Achak, M.; Bakasse, M.; el Mhammedi, M.A. Electrochemical Impedance Spectroscopic Investigation in Detecting 2,4-Dinitrophenylhydrazine Using Catalytic Effect of Copper at Glassy Electrode. *Electroanalysis* **2016**, *28*, 2965–2971. [CrossRef]
41. Peng, X.; Wang, Y.; Luo, Z.; Zhang, B.; Mei, X.; Yang, X. Facile Synthesis of Fluorescent Sulfur Quantum Dots for Selective Detection of p-Nitrophenol in Water Samples. *Microchem. J.* **2021**, *170*, 106735. [CrossRef]
42. Kovtyukhova, N.; Perea-López, N.; Terrones, M.; Mallouk, T. Atomically Thin Layers of Graphene and Hexagonal Boron Nitride Made by Solvent Exfoliation of Their Phosphoric Acid Intercalation Compounds. *ACS Nano* **2017**, *11*, 6746–6754. [CrossRef] [PubMed]
43. Ji, J.; Jia, Y.; Wu, W.; Bai, L.; Ge, L.; Gu, Z. A Layer-by-Layer Self-Assembled Fe_2O_3 Nanorod-Based Composite Multilayer Film on ITO Anode in Microbial Fuel Cell. *Colloids Surf. A Physicochem. Eng. Asp.* **2011**, *390*, 56–61. [CrossRef]
44. Elzbieciak, M.; Kolasińska, M.; Zapotoczny, S.; Krastev, R.; Nowakowska, M.; Warszyński, P. Nonlinear Growth of Multilayer Films Formed from Weak Polyelectrolytes. *Colloids Surf. A Physicochem. Eng. Asp.* **2009**, *343*, 89–95. [CrossRef]